International Journal of Informatics and Data Science Research
ISSN 2997-3961 (Online)
Vol. 2, No. 9, Sep 2025,
Available online at: https://scientificbulletin.com/index.php/IJIDSR

Design and Simulation of Fluxgate Sensor Drive Electronics for Satellite Communications

Stanislaus Kaosoluchukwu Ogbuokebe [1], Frederick Alapa [2], Nwanneka Ibekwe [3], Abdulmalik Ogohi [4], Oluwatosin Sunkanmi Aremo [5]
[1,2,3,4,5] Center for Satellite Technology Development (CSTD), National Space Research & Development Agency (NASRDA), Obasanjo Space Center, Airport Road, Abuja, Nigeria

Article information:
Manuscript received: 4 Jul 2025; **Accepted:** 10 Aug 2025; **Published:** 08 Sep 2025

Abstract: Fluxgate sensor provides very good resolution and accuracy for measuring the Earth's magnetic field, which is critical to comprehend space weather. Fluxgate sensor drive electronics for satellite communications employ an oscillating signal to periodically saturate and unsaturate a magnetic core material, producing a distinctive voltage at the output of the sense coil that changes with the external magnetic field. This paper describes the design and simulation of fluxgate sensor drive electronics, which can be used to drive the excitation coil in fluxgate magnetometer sensor (FMS). The excitation coil's electronics circuit consists of a drive oscillator, frequency divider, and voltage to current converter. In order to achieve the aim of this work, the software that was used for the simulations was based on the NI Circuit Design Suite 11.0 from the National Instruments. This is due to the versatile nature of this software. Several simulations were performed to find the best excitation frequency required to saturate the fluxgate magnetic core material. The first analysis step carried out was the evaluation of the optimum excitation frequency and current value, which guarantees the ferromagnetic core material to saturate a given geometrical dimension of the excitation coil. By carrying out the simulations using different excitation frequencies, a peak current of 29.3mA was observed to be sufficient to drive the chosen excitation coil with a 5 kHz square wave.

Keywords: Fluxgate sensor, Excitation coil, NI Circuit Design Suite, magnetic permeability, Satellite communication.

1.0 Introduction

The Earth has a varying magnetic field which comprises of an intense radiation and plasma zones, primarily due to the action of the charged particles of the solar rays impinging on the field (Waheed and Rehman, 2011; Mann *et al.*, 2011). The maximum magnetic field that the magnetic field sensor can experience in space is about ±60000nT (Lu and Huang, 2015) and a resolution on the order of about 10 pT (Korepanov and Marusenkov, 2012; Tumanski, 2013). Earth's magnetic field monitoring is essential in order to predict the occurrence of the major disturbances on the solar terrestrial environment (Yousif, 2011). The major disturbances on the solar terrestrial system include the geomagnetic storms, geomagnetic sub-storms, sudden commencement, and geomagnetic pulsations (Miles *et al.*, 2013; Matsuoka *et al.*, 2013). These disturbances reach the surface of the Earth from the solar terrestrial system through the magnetosphere (Miles *et al.*, 2013). The Earth's

magnetosphere is formed as a result of the magnetic field mapping together with the close intense of plasma (plasmasphere and other plasma regions) and interplanetary magnetic field (the nearby solar terrestrial environment) (Yousif, 2011; Trishchenko and Garand, 2012; Matsuoka *et al.*, 2013).

Magnetic storm (also called geomagnetic storm) is a worldwide disturbance of geomagnetic field (Earth's magnetic field). Magnetic storms can cause significant damage across the world with a single event (Baumjohann *et al.,* 2010). Severe geomagnetic storms can disrupt the operation of electricity power transmission systems and critical space-based infrastructures. A geomagnetic storm that damages the electric power grid would not only affect the energy sector but also the transportation, communications, banking, and finance sectors of a region affected by the geomagnetic storm (Baumjohann *et al.*, 2010).

Magnetometer is an instrument used to monitor, measure and record the three components of the Earth's magnetic field at the geomagnetic observatory. The three components of the Earth's field are the horizontal component (H), the declination component (D), and the downward component (Z). Earth's magnetic field data from ground-based magnetometer observatories are used to investigate the effects of geomagnetic storm. Fluxgate magnetometer has greatly contributed to the ongoing extensive research work dedicated to the explanation of some of the complex phenomena related to geomagnetic storm and solar terrestrial system (Benkhoff *et al.*, 2010).

Fluxgate based magnetometers are commonly used for measuring Direct Current (DC) (Lv and Liu, 2013) or low frequency Alternating Current (AC) magnetic fields (He and Shiwa, 2014; Can and Topal, 2015). Fluxgate sensors usually work on the second harmonic principle (Lv and Liu, 2013) and close-loop configuration (Matsuoka *et al.*, 2013). When the excitation current from the excitation coil's electronics is applied to the excitation coil, a lock-in amplifier (that is, phase sensitive detector and amplifier) is used to extract the second harmonic of the induced voltage from the output of the sensing (pick-up) coil of the FMS (Miles *et al.*, 2013; Lv and Liu, 2014). The amplitude of the induced second harmonic signal in the pick-up coil is proportional to the target magnetic field (Lv and Liu, 2013; Lu and Huang, 2015). In the conventional fluxgates sensor design, in order to avoid high frequency noise in the signal output of the lock-in amplifier, a low pass filter is usually employed while the output signal is used as feedback (Matsuoka *et al.*, 2013). This feedback serves to improve the linearity of the response and increases the measurement range (Lu and Huang, 2015).

In this research, excitation coil's electronics is investigated for the improved performance of FMS. The name fluxgate is clearly derived from the action of the magnetic core gating flux "in and out" of the sensing (pick-up) coil (Butta, 2012). Excitation coil's electronics provide electrical signals to an excitation coil so as to create a magnetic field, which can be used in applications like sensing, power transfer, and medical stimulation. The electronics circuit can produce different types of excitation signal, such as alternating current (AC) in form of sinusoidal, triangular, pulsed or direct current (DC) current or voltage. They are usually designed to optimize the performance, sensitivity, and safety in their respective applications by considering factors like magnetic field intensity, power consumption, and insulation.

2. LITERATURE REVIEW

The operation principle of Fluxgate Magnetometer Sensor (FMS) is based on the periodic saturation of a ferromagnetic core material (Zhang *et al.,* 2010; Solorzano, 2013). The permeability of the ferromagnetic material is modulated based on the *B-H* curve of the magnetic material (Suitella *et al.*, 2011), between the permeability of air and the absolute permeability of the magnetic material with a periodic excitation field at certain frequency (Ripka *et al.,* 2010; Bae *et al.*, 2013). Figure 1 shows the principle of operation of a ring and

rod core geometries for a parallel type configuration fluxgate magnetometer. The winding through which the excitation coil's electronics current is applied is placed around the magnetic core (Weiss *et al,* 2011; Bae *et al.,* 2013) with the coils wound in such a way that the induced magnetic fields within the core are in opposite directions (Ripka, 2010). The excitation current required to drive the magnetic core into saturation should be large enough, typically, with currents larger in magnitude than theoretically necessary (Tumanski, 2013; Indrasari *et al,* 2012). The pick-up coil winding that encircles the magnetic core is normally used to obtain the output signal.

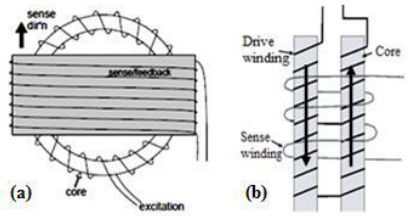

Figure 1: Fluxgate Sensor Architecture (Evans, 2006).

The excitation principles of FMS are shown in Figure 2, with the excitation voltage waveform applied to the excitation coil in Figure 2(a), excitation current waveform, illustrating when the magnetic core saturates (Evans, 2006) in Figure 2(b), and finally the sensing coil output voltage waveform, which corresponds to the ambient magnetic field in Figure 2(c). The frequency of this sensing coil output voltage is twice the frequency of the excitation signal due to flux change detection, which occurs at twice (two flux collapsing during each cycle) the frequency of the excitation signal (Weiss *et al,* 2010).

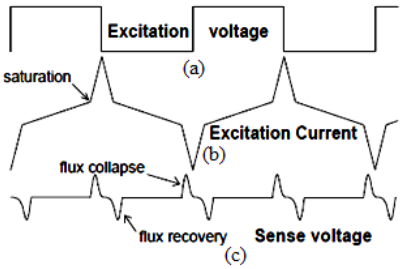

Figure 2: Fluxgate Sensor Waveform (Evans, 2006).

Driving the excitation coil and detecting the sensing coil signal in FMS require careful design of the excitation coil's and detection electronics circuits (Baschirotto *et al.,* 2010; Velasco *et al.,* 2011). In most literatures, the excitation circuits for FMS are typically based on a sinusoidal (Zorlu *et al.,* 2010), triangular (Baschirotto *et al.,* 2010) or pulsed excitation (Waheed and Rehman, 2011). The pulsed excitation is the most easier to generate than sinusoidal or triangular excitation (Ripka, 2001) and represents a trade-off between the sensitivity and power consumption (Cui, 2013). Also, a pulsed excitation reduces power consumption at the expense of low sensors sensitivity (Baschirotto *et al.,* 2010; Cui, 2013). The block diagram of FMS principles is shown in Figure 3. In order to periodically saturate the ferromagnetic core material, the square wave signal from the excitation coil's electronics, with required frequency and current is fed into the sensor's excitation coil. The sensing coil of the FMS detects the signal by the rising and falling edges of core magnetizing current (shown in Figure 2(c)). In principle, the second harmonic FMSs produce the highest sensitivity and the lowest noise. The sensing coil output signal is usually fed into a pre-amp with mild tuning to the second harmonic (*2f*) of the excitation frequency (Lu and Huang, 2015). The information on the external magnetic field is then extracted by using synchronous demodulation technique (Miles *et al.,* 2013) and also demodulated using a phase sensitive detection technique (Tumanski, 2013).

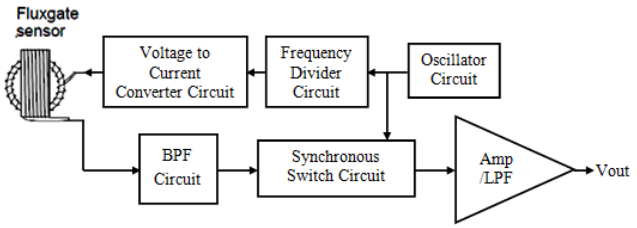

Figure 3: Typical Second Harmonic Demodulator Scheme

3. MATERIALS AND METHODOS

As mentioned earlier, driving the excitation coil and extracting the magnetic field information from the sensing coil of FMS require careful design of the excitation coil's and detection electronics circuits (Baschirotto *et al.*, 2010; Velasco *et al.*, 2011). The software that was used for the simulations is based on the NI Circuit Design Suite 11.0 from the National Instruments (NI, 2010). Several simulations were performed to find the best excitation frequency needed to saturate the required fluxgate sensor magnetic core material. The first analysis step was to evaluate the optimum excitation frequency and current value that guarantees the ferromagnetic material to saturate, for a given geometrical dimension of the excitation coils. Although, Frequency generator circuits can be designed using different electronics components such as operational amplifier, transistors, hex inverters, and so on. In order to achieve the aim of this research, the Integrated Circuit (IC) CD4069 is a CMOS logic chip having six independent inverters has been chosen to design a simple square wave generators as shown in Figure 4. This was achieved by connecting two hex inverters in series. The pulse generator was designed to produce a frequency of 10kHz and a 50% duty cycle signal. A duty cycle different from 50% could compromise the demodulation of the signals produced by the pick-up coil (Baschirotto *et al.*, 2005). The frequency determined by $R_{12,}$ R_{13} and C_5 is calculated (Fairchild, 2002) as:

$$F_{exc} = \frac{1}{1.39\ x\ R_1\ x\ C_1} \quad (1)$$

Where F_{exc} is the frequency in Hz, $R_{12,}$ and R_{13} are the timing resistor in ohms while C_5 is the timing capacitor in Farad.

As shown in Figure 4, the circuit uses a few components such as three resistors with R_{12} and R_{13} used as timing resistor and a capacitor C_5 and consumes less power. The capacitor here is a circuit element that stores charge and the total charge is proportional to voltage. As stated earlier, the output frequency of this square wave oscillator stage depends on the three components R_{12}, R_{13}, and C_5. Varying the value of any of these three components will vary the output frequency.

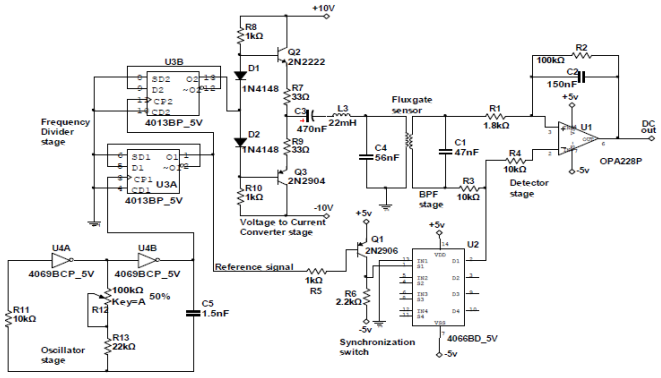

Figure 4: Full Schematic Diagram of the Developed Analog Fluxgate Magnetometer

Following the square wave frequency generator stage is the Frequency divider circuit stage, which was designed by selecting a dual flip-flop IC CD4013. The dual flip-flop IC consists of two flip-flops, which can be used in an independent manner (Fairchild, 2002). Inputs D1 & D2 pins are meant for data input, which can be either logic 1 or 0. CP1 and CP2 are the clock input for Flip-Flops 1 & 2. The SD1 and CD1 as well as SD2 and CD2 are Set and Reset pins of the respective Flip Flops (Fairchild, 2002). CD4013 is a dual D-type flip-flop, which was configured to divide the incoming pulse frequency from the square wave of Figure 4. In order to configure IC 4013 as a Frequency divider, the complement pin (~Q) is feedback to the data input D1 of each flip-flop. The feedback signal of the complement (~Q) pin to the data input divides the clock signal frequency by half. Connecting the next Flip flop in such manner provides a signal of F/4 of the original frequency of the pulse obtained from the square wave oscillator. Thus, we can obtain F/8, F/16 signals by connecting the Flips-Flops in continuous sequence.

The frequency divider output produces an analog output voltage with very low excitation current, which cannot be directly used to drive the FMS magnetic core into saturation. The oscillator and the frequency divider can only produce a few tens of milli-amperes at most, while the sensor's magnetic core requires higher milli-amperes. Hence, there is need for current amplification by using power transistors. In order to achieve this in this research, a complementary emitter-follower is employed for efficient bipolar current amplification. As shown in Figure 4, a low-noise class-AB power amplifier with NPN and PNP transistors Q2 and Q3 respectively was utilized. The two transistors Q2 and Q3 were configured as a complementary emitter-follower. There are many amplifier circuits suitable for voltage-to-current conversion in fluxgate sensor design, but the class-AB amplifier chosen can provide sufficient current required for sensor the core saturation (Karthik, 2013).

As shown in Figure 4, resistor R8 and diode D1 biased the NPN transistor Q2 while D2 and R10 biased the transistor Q3. The values of the biasing resistors R8 and R10 are calculated as:

$$R_8 = \frac{V_{CC} - V_{BE}}{I_{REF}} \quad (2)$$

Where R8 is the Q2 bias resistor. Biased resistors R8 and R10 values are equal and set the operating current for the output of the transistors. V_{cc} is the supplied voltage, V_{be} is the emitter-base voltage and I_{REF} is the transistor base bias current, which flows from the supplied voltage through R8 to the base of the transistor Q2. As Resistors R8 and R10 are equal in values and set the operating current for the output of the transistors. The values of the emitter biasing resistors R7 and R9 are calculated as:

$$R_7 = \frac{V_{CC}}{I_0} \ln\left(\frac{I_{REF}}{I_0}\right) \quad (3)$$

Where R7 is an emitter bias resistor and R7 is equal to R9. V_{cc} is the supplied voltage, I_o is the output current, and I_{REF} is the transistor base bias current.

The two diodes D1 and D2 serve to bias the transistors Q2 and Q3 and reduce the cross-over distortion that occurs when the input waveform crosses zero. Without these diodes, the oscillator output would have to swing 1.4V to turn one transistor on and then bring the other transistor off.

In order to apply the signal from the excitation coil's electronics to the FMS excitation coil, there is need for a coupling capacitor, which serves to isolate the AC signal from any DC bias voltages. Therefore, the chosen coupling capacitor must have the appropriate value. Capacitor C3 served to block the DC component of the current source from reaching the excitation resonant circuit forms by capacitor C4 and the FMS excitation coil. The equation

employed to calculate the value of the coupling capacitor C3 is:

$$C_3 = \frac{1}{3.2\ x\ f_{exc}\ x\ R_{coil}} \quad (4)$$

Where C3 is the capacitance in Farads, and f_{exc} is the excitation signal frequency in Hertz. R_{coil} is the impedance on the load side of the capacitor which in this case is the excitation coil resistance in Ohms.

As shown in Figure 4, when transistor Q2 is turned on, capacitor C3 is charged smoothly as the charging current is limited by inductor L3. The main function of the inductor L3 is to limit the current drawn from the source for the fluxgate excitation current. This was achieved by using a high impedance (larger than the fluxgate sensor) inductor, which operates in the non-saturated mode. In the non-saturated state, the high impedance of the inductor limits the current flowing from the source to the excitation circuit.

4. RESULTS AND DISCUSSIONS

As presented in the block diagram of Figure 3, FMS system employed in this research composed mainly of seven different blocks. The drive electronics consists of square wave oscillator, frequency divider, and current amplifier while the sense electronics include the band pass filter, synchronous detector, and amplifier with low pass filter. After carrying out the simulations using the circuit shown in Figure 4, a peak current of 29.3mA turned out to be sufficient to drive the FMS excitation coil with the geometrical dimensions of the magnetic cores. The simulation results are presented in Figure 5.

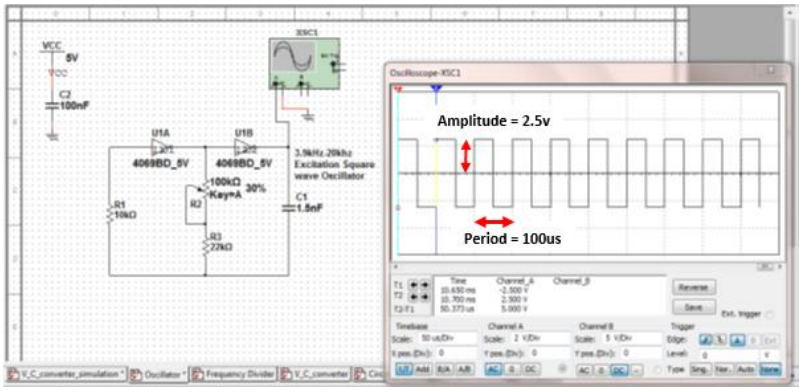

Figure 5: 5 kHz Square Wave Excitation Frequency Circuit Simulation

After an iterative process of design optimization, the excitation frequency selected is a 10 kHz square wave as shown in the Oscilloscope view of Figure 5. Oscilloscopes are useful for looking at things that we could not measure with a multimeter during very fast changes in voltage over time. The graph obtained stretches from left side to the right side of the screen and is usually a graph of Voltage versus Time, where voltage is measured along the y axis and time along the x. As seen on the oscilloscope screen, volts/div indicates the amount of voltage represented by each vertical increment of grid overlay on the screen, while the time/div indicates the amount of time represented by each horizontal increment of the grid overlay on the screen.

$$\frac{Volts}{div} = 2V$$

$$\frac{time}{div} = 50\mu s$$

Therefore, the amplitude of the square waveform shown on the Oscilloscope is the difference between the height of the peaks of the wave and the wave's equilibrium (the value

which the wave is oscillating around). In this case, the wave has been centered to oscillate around the center horizontal grid line. The distance between this equilibrium line and either the high or low peak of the wave is 2.5 vertical grid divisions (see the red arrows). Since volts/div is set to 2V, 1.25 grid divisions on the oscilloscope equals 2.5V, so the amplitude of the oscillator waveform is 2.5V.

More so, the frequency of the waveform seen on the oscilloscope is the number of times per second that a wave repeats its shape. It's not usually possible to directly measure the frequency of waveform on the oscilloscope, but we can measure period, which is a closely related parameter. Therefore, the period of a wave is the amount of time it takes to complete one full cycle. As indicated on the oscilloscope screen of Figure 5, one cycle is completed in 2 horizontal grid divisions. As indicated in the bottom of the screen, the time/div has been set to 50µs, so 2 divisions equals 100µs (0.0001 seconds). Using the relationship,

$$frequency = \frac{1}{period} \quad (5)$$

The period of the signal is calculated to be 10,000cycles/second (or 10,000Hz or 10kHz).

As the frequency divider output current is very low and cannot be directly used to drive the FMS magnetic core to saturation. Hence, there is need for current amplification, which was achieved and simulated in this research by using a complementary emitter-follower circuit as presented in Figure 4 while the simulated output result is presented in Figure 6.

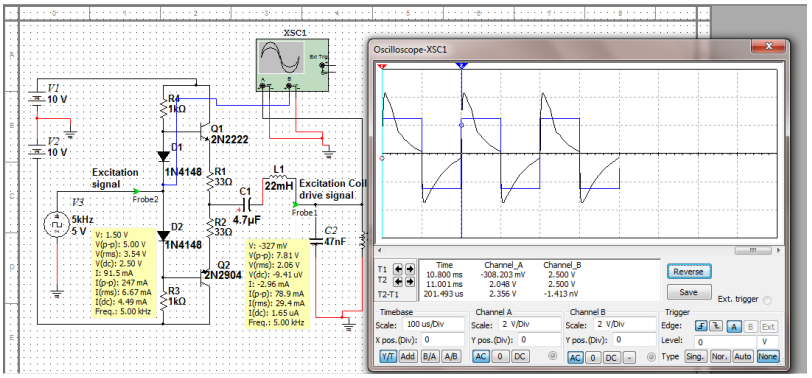

Figure 6: Simulation Results of the Voltage-to-Current Converter

As seen in Figure 6, it can be noticed that the current waveform from the current amplifier is highly distorted. This is due to the magnetic core saturation. The magnetic core reach saturation level during the first half (positive) cycle of the excitation voltage waveform, and began to fall during the second (negative) half cycle. The frequency of the voltage-to-current converter circuit is 5kHz. This is due to the frequency divider employed between the oscillator and the current amplifier. The amplitude of the excitation current waveform is 2.5V. The time/div has been set to 100µs, so 2 divisions equals 200µs (0.0002 seconds). Using equation (5), the period of the signal is therefore calculated to be 5,000 cycles/second (or 5,000Hz or 5kHz).

5. CONCLUSION

In conclusion, the fluxgate sensor drive electronics serve as the foundation for the effective operation of a FMS for satellite communications, by providing the means to interact with the magnetic core material and generate the measured signals. It therefore influences every aspect of the sensor's performance. The simulation of the excitation coil's electronics has been designed and simulated using NI Circuit Design Suite 11.0 from the National Instruments. The first analysis step was carried out by evaluating the optimum excitation frequency and current value that guarantees the ferromagnetic core material saturation. By

carrying out simulations using different excitation frequencies, a peak current of 29.3mA was observed to be sufficient to drive the excitation coil based on the geometrical dimensions of the magnetic core with the excitation frequency of 5 kHz square wave. The designed and simulated excitation coil's electronics can precisely control the excitation signal, determining the sensor's performance, sensitivity, and power consumption. The excitation circuit's design directly impacts the magnetometer's sensitivity. Finally, it was noticed that, by tuning the excitation coil's electronics parameters, like amplitude and frequency, the sensor's noise can be minimized while the overall performance can be improved.

REFERENCES

1. Bae, S.; Hong, Y.K.; Lee, J.; Park, J.; Jalli, J.; Abo, G.S.; Kwon, H.M. and Jayasooriya, C.K.K. (2013). Pulsed ferrite magnetic field generator for through-the-earth communication systems for disaster situation in mines. *Journal of Magnetics, 18(1)/*43-49.
2. Baschirotto, A.; Dallago, E.; Ferri, M.; Malcovati, P.; Rossini, A. and Venchi, G. (2010). A 2D micro-fluxgate earth magnetic field measurement system with fully automated acquisition setup, *Measurement, 43*(1)/46-53.
3. Baumjohann, W. *et al.* (2010). Magnetic field investigation of Mercury‟s magnetosphere and the inner heliosphere by MMO/MGF, *Planet Space Science, 58(2)*/279–286.
4. Benkhoff, J.; Casteren, J.V.; Hayakawa, H.; Fujimoto, M.; Laakso, H.; Novara, M.; Ferri, P.; Middleton, H.R. and Ziethe, R. (2010). BepiColombo-Comprehensive exploration of Mercury: Mission overview and science goals, *Planet Space Science, 58(1)*/2–20.
5. Butta, M. (2012). *Orthogonal Fluxgates, Magnetic Sensors - Principles and Applications*, Dr Kevin Kuang (Ed.). Shanghai: InTech.
6. Can, H. & Topal, U. (2015). Design of ring core fluxgate magnetometer as attitude control sensor for low and high orbit satellites. *Journal of Superconductivity and Novel Magnetism. 28*/1093-1096.
7. Cui, Z. J. (2013). Design of a novel excitation circuit for low perming error fluxgate. *Advanced Materials Research, 748*/859-863.
8. Evans, K. (2006). Fluxgate magnetometer explained. *Invasens,* http://www.invasens.co.uk/FluxgateExplained.PDF Accessed 10 November 2009.
9. Fairchild Semiconductor (2002). CD4049 Hex Inverting Buffer Manual. Fairchild Semiconductor Corporation.
10. He and Shiwa, (2014). A magnetic sensor with amorphous wire. *Sensors. 14*/10644 – 10649.
11. Indrasari, W.; Djamal, M.; Srigutomo, W. and Ramli (2012). A magnetic distance sensor with high sensitivity based on double secondary coil of fluxgate. *IOSR Journal of Applied Physics (IOSR-JAP), 2(5)/*29-35.
12. Karthik, P. (2013). A CMOS Analog Front-End Circuit for Micro-Fluxgate Sensors. A M.Sc. Thesis (Unpublished). Arizonal State University.
13. Korepanov, V. and Marusenkov, A. (2012). Flux-gate magnetometers design peculiarities. *Survey Geophysics, 33*/1059-1079.
14. Lu, C. C. and Huang, J. (2015). A 3-Axis miniature magnetic sensor based on a planar

fluxgate magnetometer with an orthogonal fluxguide. *Sensors, 15*/14727-14744.

15. Lv, H. and Liu, S. (2014). Design and fabrication of low power consumption micro fluxgate sensor. *Sensors and Transducers, 182(11)*/22-27.
16. Mann, I. R., Rae, I. J., Ozeke, L. G., Miles, D. M., and Yau, A. W. (2011). Plasma and Radiation *In Molniya Orbit (PRIMO) Science Objective and User's Needs Definition Document, Technical report*, Universities of Alberta, Edmonton, Canada.
17. Matsuoka, A.; Shinohara, M.; Tanaka, Y.M.; Fujimoto, A. and Iguchi, K. (2013). Development of fluxgate magnetometers and applications to the space science missions. *An Introduction to Space Instrumentation*, Edited by K. Oyama & C. Z. Cheng, 217–225.
18. Miles, D.M.; Bennest, J.R.; Mann, I.R. and Millling, D.K. (2013). A radiation hardened digital fluxgate magnetometer for space applications. *Geoscience Instrumentation Methodology Data System*, *2*/213–224.
19. Ripka, P.; Butta, M.; Jie, F. and Li, X. (2010). Sensitivity and noise of wire-core transverse fluxgate. *IEEE Transactions on Magnetics, 46*/654–657.
20. Solorzano, E.F. (2013). A fluxgate magnetometer and an EMIS algorithm to study Europa‟s subsurface. *Objective Europa*, 1-9.
21. Suitella, D.Y. and Windarto, D.M.T (2011). High precision fluxgate current sensor. 1-6.
22. Trishchenko, A. P. and Garand, L. (2012). Observing polar regions from space: advantages of a satellite system on a highly elliptical orbit versus a constellation of low Earth polar orbiters, Can. *Journal of Remote Sensing*, *38*/12–24.
23. Tumanski, S. (2013). Modern magnetic field sensors: A Review. *Przegląd Elektrotechniczny*, *89*/1-12.
24. Velasco, Q. G.; Román, L. M.; Conesa, R. A. and Jeréz, F. (2011). Design of a low-consumption fluxgate transducer for high-current measurement applications. *IEEE Sensors Journal*, 11(2)/280-287.
25. Waheed, O.T. and Rehman, A. (2011). Design and development of a fluxgate magnetometer for small satellites in low earth orbit. *Journal of Space Technology*, 1(1)/78-82.
26. Weiss, E. and Paperno, E. (2011). Noise investigation of the orthogonal fluxgate employing alternating direct current bias. *Journal of Applied Physics*, 109/529.
27. Yousif, S.M.E. (2011). *Data Analysis*. MAGDAS School, Redeemer‟s University, Mowe, Ogun State, Nigeria.
28. Zhang, Y.; Steiger, M.; Hibbs, A.D.; Grimm, R.E. and Sprott, T.A. (2010). Dual-mode, fluxgate-induction sensor for UXO detection and discrimination, *Journal of Environmental Engineering and Geophysics. 15(2)*/51–64.